

# Quasiparticle Structure in Antiferromagnetism around the Vortex and Nuclear Magnetic Relaxation Time

Mitsuaki Takigawa,\* Masanori Ichioka, and Kazushige Machida  
*Department of Physics, Okayama University, Okayama 700-8530, Japan*  
 (Dated: September 28, 2018)

On the basis of the Bogoliubov-de Gennes theory for the two-dimensional extended Hubbard model, the vortex structure in  $d$ -wave superconductors is investigated including the contribution of the induced incommensurate antiferromagnetism around the vortex core. As the on-site repulsive interaction  $U$  increases, the spatial structure of charge and spin changes from the antiferromagnetic state with checkerboard modulation to that with the stripe modulation. By the effect of the induced antiferromagnetic moment, the zero-energy density of states is suppressed, and the vortex core radius increases. We also study the effect of the local density of states (LDOS) change on the site-dependent nuclear relaxation rate  $T_1^{-1}(\mathbf{r})$ . These results are compared with a variety of experiments performed on high  $T_c$  cuprates.

PACS numbers: 76.60.Pc, 74.25.Qt, 74.25.Jb, 74.25.Ha

## I. INTRODUCTION

Much attention has been focused on vortex states in various type II superconductors. We are now realizing that Fermionic excitations, or low-lying quasi-particles induced around a vortex core play a fundamental role in determining various physical properties of a superconductor and reflect sensitively the pairing symmetry.<sup>1,2,3</sup> This is particularly true for  $d$ -wave pairing case realized in high  $T_c$  cuprates. There, the contribution of nodal quasi-particles is present in the spectrum of the quasi-particles, even before applying a field.

Recently, several experiments report an “anomalous” vortex core in high  $T_c$  superconductors, which is not expected in an ordinary mixed state: (1) Hoffman, *et al.*<sup>6</sup> made an scanning tunneling microscopy (STM) observation and found a checkerboard pattern around a vortex core in Bi2212, indicating that the low energy LDOS is modified with four-site periodicity. (2) Elastic neutron scattering observes the enhancement of the scattering peaks associated with incommensurate antiferromagnetism (AFM) modulation in  $\text{La}_{2-x}\text{Sr}_x\text{CuO}_4$  (LSCO)<sup>7,8,9</sup> under small fields ( $\sim$  a few T) compared with  $H_{c2}$ . The magnetic moment is found to be increased by a small field. (3) Recent  $\mu\text{SR}$  measurement detects a static moment in the vortex state in under-doped  $\text{YBa}_2\text{Cu}_3\text{O}_{7-\delta}$  (YBCO).<sup>10</sup> Kadono, *et al.*<sup>11</sup> also demonstrate that the spontaneous moment is induced by a small field around a vortex core on LSCO. (4) Finally, site-selective nuclear magnetic resonance (NMR) experiments<sup>12,13</sup> show that nuclear magnetic relaxation time  $T_1$  at the core site becomes longer as  $T$  decreases, indicating the lack of LDOS at low  $T$ . The above facts strongly suggest that in high  $T_c$  superconductors the vortex core is quite different from what we expect in “normal”  $d$ -wave vortex,<sup>3</sup> namely a picture that under a small applied field the spatially modulated AFM moments are induced centered around a vortex core and simultaneously the zero-energy peak (ZEP)<sup>14</sup> at a core is suppressed. This picture is also consistent with the ear-

lier STM observations which show an “empty core”, namely the absence of the ZEP at the core site.<sup>15</sup> The AFM around the vortex<sup>16,17,18,19,20,21,22,23,24,25,26</sup> was also studied theoretically in SO(5) model,<sup>16,17</sup> QED<sub>3</sub> model,<sup>18</sup>  $t$ - $J$  model,<sup>19,20,21</sup> and Hubbard model.<sup>23,24,25,26</sup>

Quite recently, two new NMR imaging experiments<sup>27,28</sup> on the  $T$ -dependence of  $T_1$  are reported: Kakuyanagi, *et al.*<sup>27</sup> show in  $\text{Tl}_2\text{Ba}_2\text{CuO}_6$  that as lowering  $T$ ,  $1/(T_1T)$  at a core site increases divergently toward a temperature  $T_M$  below  $T_c$  and then decreases at lower  $T$ . This is contrasted with  $1/(T_1T)$  at other sites which exhibit a monotonic decrease below  $T_c$ . This result suggests that below  $T_M$  the local magnetism appears exclusively at a vortex core site and other sites stay in the normally expected  $d$ -wave state. Mitrović, *et al.*<sup>28</sup> observe a similar divergent behavior in  $1/(T_1T)$  of  $\text{YBa}_2\text{Cu}_3\text{O}_7$  at the core site where the crossover temperature  $T_M$  is quite low, and  $1/(T_1T)$  at the outside sites of the core show a constant at low  $T$ . The implication of these experiments is twofold: The ZEP in  $d$ -wave vortex core must be present at  $T_M < T < T_c$  and in some  $H$  region, and its contribution enhances  $1/(T_1T)$  in this temperature region. Below  $T_M$ , the field induced local AFM must exist, which is to remove the ZEP, giving rise to a suppression of  $1/(T_1T)$  at lower  $T$ . These new experiments further enforce the above picture of the AFM-induced vortex core state.

Here we explore a possibility of the induced incommensurate AFM moment around a vortex in  $d$ -wave pairing state. It is quite possible because (A) in a  $d$ -wave vortex state the zero-energy quasi-particles produced at a vortex core are readily available for the magnetism and (B) these quasi-particles are under strongly correlated environment in cuprates, where the AFM state appears near half filling next to the superconducting phase. Therefore, based on these experimental facts we are led to investigate how two orders;  $d$ -wave superconducting order with vortices and the modulated magnetic order can be influenced in order to compromise mutual competing effects.

The purposes of this paper are to study detailed prop-

erties of the vortex core under the possible magnetic order, in particular on the quasi-particle structure and to calculate the site-selective  $T_1(\mathbf{r})$  which turns out to be a good probe for examining the quasi-particles at a vortex core. This study is not only one of our continuous efforts on the vortex problem but also associated with our stripe problem.<sup>29,30</sup> When the stripe structure is formed, the doped carriers are accommodated neatly at the stripe region, ultimately relating to the mechanism of the high  $T_c$  superconductivity. Therefore, we consider the case when the induced AFM around vortex is not in commensurate AFM structure<sup>25,26</sup> with the ordering vector  $\mathbf{Q} = (\pi, \pi)$ , but in incommensurate spin and charge structure, where the spin ordering vector is given by  $\mathbf{Q} = (2\pi(\frac{1}{2} - \epsilon), \pi)$  or  $\mathbf{Q} = (\pi, 2\pi(\frac{1}{2} - \epsilon))$ . Following the neutron scattering results,<sup>7,8,9</sup>  $\epsilon = \frac{1}{8}$  at hole filling  $n_h \sim \frac{1}{8}$ , meaning the eight site periodic spin structure. In this case, the charge structure characterized by the ordering vector  $2\mathbf{Q}$  shows four site periodic oscillation, which is consistent with the STM observation.<sup>6</sup>

The arrangement of this paper is as follows: After introducing the model Hamiltonian which allows us to describe two possible orderings of superconductivity and magnetism in an equal footing, namely, the so-called extended Hubbard Hamiltonian, we set up the Bogoliubov-de Gennes (BdG) equation on a lattice, and a formula for the LDOS and  $T_1(\mathbf{r})$  in Sec. 2. The basic vortex properties, including the amplitude of the induced moment, the local charge distribution, and the Fourier component are studied in Sec. 3. We discuss the LDOS in Sec. 4, and evaluate the  $T$ -dependence and site-dependence of  $T_1(\mathbf{r})$  in Sec. 5. The final section is devoted to conclusion and discussion. Some of the results are briefly reported in Refs. 24 and 31.

## II. BOGOLIUBOV-DE GENNES THEORY ON EXTENDED HUBBARD MODEL

We begin with an extended Hubbard model on a two-dimensional square lattice, and introduce the mean fields  $n_{i,\sigma} = \langle a_{i,\sigma}^\dagger a_{i,\sigma} \rangle$  at the  $i$ -site, where  $\sigma$  is a spin index and  $i = (i_x, i_y)$  and  $\Delta_{\hat{e},i,\sigma} = \langle a_{i,-\sigma} a_{i+\hat{e},\sigma} \rangle$ . We assume a pairing interaction  $V$  between nearest-neighbor (NN) sites. This type of pairing interaction gives  $d$ -wave superconductivity.<sup>32,33,34</sup> Thus, the mean-field Hamiltonian under  $H$  is given by

$$\mathcal{H} = - \sum_{i,j,\sigma} \tilde{t}_{i,j} a_{i,\sigma}^\dagger a_{j,\sigma} + U \sum_{i,\sigma} n_{i,-\sigma} a_{i,\sigma}^\dagger a_{i,\sigma} + V \sum_{\hat{e},i,\sigma} (\Delta_{\hat{e},i,\sigma}^* a_{i,-\sigma} a_{i+\hat{e},\sigma} + \Delta_{\hat{e},i,\sigma} a_{i,\sigma}^\dagger a_{i+\hat{e},-\sigma}^\dagger) \quad (1)$$

where  $a_{i,\sigma}^\dagger$  ( $a_{i,\sigma}$ ) is a creation (annihilation) operator, and  $i + \hat{e}$  represents the NN site ( $\hat{e} = \pm\hat{x}, \pm\hat{y}$ ). The transfer

integral is expressed as

$$\tilde{t}_{i,j} = t_{i,j} \exp[i \frac{\pi}{\phi_0} \int_{\mathbf{r}_i}^{\mathbf{r}_j} \mathbf{A}(\mathbf{r}) \cdot d\mathbf{r}], \quad (2)$$

with the vector potential  $\mathbf{A}(\mathbf{r}) = \frac{1}{2} \mathbf{H} \times \mathbf{r}$  in the symmetric gauge, and the flux quantum  $\phi_0$ . The external field is introduced as the so-called Peierls phase factor.

We assume the following hopping integrals  $t_{ij}$ : For the NN pairs  $(i, j)$ ,  $t_{i,j} = t$ . For the next-NN pairs situated on a diagonal position on the square lattice,  $t_{i,j} = t'$ . For the third-NN pairs, which are situated along the NN bond direction,  $t_{i,j} = t''$ . To reproduce the Fermi surface topology of cuprates, we set  $t' = -0.12t$  and  $t'' = 0.08t$ .<sup>35</sup> We consider mainly the pairing interaction  $V = -2.0t$ . The essential results of this paper do not significantly depend on the choice of these parameter values.

In terms of the eigenenergy  $E_\alpha$  and the wave functions  $u_\alpha(\mathbf{r}_i)$  and  $v_\alpha(\mathbf{r}_i)$  at the  $i$ -site, the BdG equation is given by

$$\sum_j \begin{pmatrix} K_{\uparrow,i,j} & D_{i,j} \\ D_{i,j}^\dagger & -K_{\downarrow,i,j}^* \end{pmatrix} \begin{pmatrix} u_\alpha(\mathbf{r}_j) \\ v_\alpha(\mathbf{r}_j) \end{pmatrix} = E_\alpha \begin{pmatrix} u_\alpha(\mathbf{r}_i) \\ v_\alpha(\mathbf{r}_i) \end{pmatrix}, \quad (3)$$

where  $K_{\sigma,i,j} = -\tilde{t}_{i,j} + \delta_{i,j}(Un_{i,-\sigma} - \mu)$  with the chemical potential  $\mu$ ,  $D_{i,j} = V \sum_{\hat{e}} \Delta_{i,j} \delta_{j,i+\hat{e}}$  and  $\alpha$  is an index of the eigenstate.<sup>32,33</sup>

We study the case of the square vortex lattice where the NN vortex is located in the direction of  $45^\circ$  from the  $a$ -axis, which is known to be a stable vortex configuration. The unit cell in our calculation is the square area of  $N_r^2$  sites where two vortices are accommodated. Then, the magnetic field is given by  $H = 2\phi_0/(aN_r)^2$  with the lattice constant  $a$ . Thus, we denote the field strength by  $N_r$  as  $H_{N_r}$ . We consider the area of  $N_k^2$  unit cells. By introducing the quasi-momentum of the magnetic Bloch state,  $\mathbf{k} = (2\pi/aN_rN_k)(l_x, l_y) : (l_x, l_y = 1, 2, \dots, N_k)$ , we set  $u_\alpha(\mathbf{r}) = \tilde{u}_\alpha(\mathbf{r})e^{i\mathbf{k} \cdot \mathbf{r}}$ ,  $v_\alpha(\mathbf{r}) = \tilde{v}_\alpha(\mathbf{r})e^{i\mathbf{k} \cdot \mathbf{r}}$ . Then, the eigenstate of  $\alpha$  is labeled by  $\mathbf{k}$  and the eigenvalues obtained by solving Eq. (3) within a unit cell. The periodic boundary condition is given by the symmetry for the translation  $\mathbf{R} = l_x \mathbf{R}_x^0 + l_y \mathbf{R}_y^0$ , where  $\mathbf{R}_x^0 = (aN_r, 0)$  and  $\mathbf{R}_y^0 = (0, aN_r)$  are unit vectors of the unit cell for our calculation. Then, the translational relation is given by  $\tilde{u}_\alpha(\mathbf{r} + \mathbf{R}) = \tilde{u}_\alpha(\mathbf{r})e^{i\chi(\mathbf{r}, \mathbf{R})/2}$  and  $\tilde{v}_\alpha(\mathbf{r} + \mathbf{R}) = \tilde{v}_\alpha(\mathbf{r})e^{-i\chi(\mathbf{r}, \mathbf{R})/2}$  with

$$\chi(\mathbf{r}, \mathbf{R}) = -\frac{2\pi}{\phi_0} \mathbf{A}(\mathbf{R}) \cdot \mathbf{r} - 2\pi l_x(l_x - l_y) + \frac{2\pi}{\phi_0} (\mathbf{H} \times \mathbf{r}_0) \cdot \mathbf{R} \quad (4)$$

in the symmetric gauge. The vortex center is located at  $\mathbf{r}_0 + \frac{1}{4}(3\mathbf{R}_x^0 + \mathbf{R}_y^0)$ .

The self-consistent conditions for the pair potential

$\Delta_{i,j}$  and the number density  $n_{i,\sigma}$  are given by

$$\Delta_{i,j} = \langle a_{j,\downarrow} a_{i,\uparrow} \rangle = \sum_{\alpha} u_{\alpha}(\mathbf{r}_i) v_{\alpha}^*(\mathbf{r}_j) f(E_{\alpha}), \quad (5)$$

$$n_{i,\uparrow} = \langle a_{i,\uparrow}^{\dagger} a_{i,\uparrow} \rangle = \sum_{\alpha} |u_{\alpha}(\mathbf{r}_i)|^2 f(E_{\alpha}), \quad (6)$$

$$n_{i,\downarrow} = \langle a_{i,\downarrow}^{\dagger} a_{i,\downarrow} \rangle = \sum_{\alpha} |v_{\alpha}(\mathbf{r}_i)|^2 (1 - f(E_{\alpha})) \quad (7)$$

with the Fermi distribution function  $f(E)$ . The charge density  $n(\mathbf{r}_i) = n_{i,\uparrow} + n_{i,\downarrow}$ , the spin density  $S_z(\mathbf{r}_i) = \frac{1}{2}(n_{i,\uparrow} - n_{i,\downarrow})$  and the staggered magnetization  $M(\mathbf{r}_i) = (-1)^{i_x+i_y} S_z(\mathbf{r}_i)$ . The  $d$ -wave order parameter at site  $i$  is

$$\Delta_d(\mathbf{r}_i) = (\Delta_{\hat{x},i} + \Delta_{-\hat{x},i} - \Delta_{\hat{y},i} - \Delta_{-\hat{y},i})/4 \quad (8)$$

with  $\Delta_{\hat{e},i} = \bar{\Delta}_{i,i+\hat{e}} \exp[i\frac{\pi}{\phi_0} \int_{\mathbf{r}_i}^{(\mathbf{r}_i+\mathbf{r}_{i+\hat{e}})/2} \mathbf{A}(\mathbf{r}) \cdot d\mathbf{r}]$ , where the singlet pairing component  $\bar{\Delta}_{i,i+\hat{e}} = \langle a_{i+\hat{e},\downarrow} a_{i,\uparrow} \rangle - \langle a_{i+\hat{e},\uparrow} a_{i,\downarrow} \rangle$ . As the induced order parameter, we can define the triplet- $d$ -wave order parameter at  $i$ -site, given by

$$\Delta_{d,i}^{\text{triplet}}(\mathbf{r}_i) = (\Delta_{\hat{x},i}^{\text{triplet}} + \Delta_{-\hat{x},i}^{\text{triplet}} - \Delta_{\hat{y},i}^{\text{triplet}} - \Delta_{-\hat{y},i}^{\text{triplet}})/4, \quad (9)$$

where we use the triplet pairing component  $\bar{\Delta}_{i,i+\hat{e}}^{\text{triplet}} = \langle a_{i+\hat{e},\downarrow} a_{i,\uparrow} \rangle + \langle a_{i+\hat{e},\uparrow} a_{i,\downarrow} \rangle$  instead of  $\bar{\Delta}_{i,i+\hat{e}}$ .

We construct the Green's functions from  $E_{\alpha}$ ,  $u_{\alpha}(\mathbf{r})$ ,  $v_{\alpha}(\mathbf{r})$  defined as

$$\begin{aligned} \hat{g}(x, x') &\equiv \begin{pmatrix} g_{11}(x, x') & g_{12}(x, x') \\ g_{21}(x, x') & g_{22}(x, x') \end{pmatrix} \\ &\equiv \begin{pmatrix} -\langle T_{\tau} [\hat{\psi}_{\uparrow}(x) \hat{\psi}_{\uparrow}^{\dagger}(x')] \rangle & -\langle T_{\tau} [\hat{\psi}_{\uparrow}(x) \hat{\psi}_{\downarrow}(x')] \rangle \\ -\langle T_{\tau} [\hat{\psi}_{\downarrow}^{\dagger}(x) \hat{\psi}_{\uparrow}^{\dagger}(x')] \rangle & -\langle T_{\tau} [\hat{\psi}_{\downarrow}^{\dagger}(x) \hat{\psi}_{\downarrow}(x')] \rangle \end{pmatrix}. \end{aligned} \quad (10)$$

with  $x \equiv (\mathbf{r}, \tau)$ . After the Fourier transformation of  $\tau$  as

$$\hat{g}(x, x') = T \sum_{\omega_n} e^{-i\omega_n(\tau-\tau')} \hat{g}(\mathbf{r}, \mathbf{r}', \omega_n), \quad (11)$$

the thermal Green's functions with the Fermionic imaginary frequency  $\omega_n = 2\pi T(n + \frac{1}{2})$  are written as

$$g_{11}(\mathbf{r}, \mathbf{r}', \omega_n) = \sum_{\alpha} \frac{u_{\alpha}(\mathbf{r}) u_{\alpha}^*(\mathbf{r}')}{i\omega_n - E_{\alpha}}, \quad (12)$$

$$g_{12}(\mathbf{r}, \mathbf{r}', \omega_n) = \sum_{\alpha} \frac{u_{\alpha}(\mathbf{r}) v_{\alpha}^*(\mathbf{r}')}{i\omega_n - E_{\alpha}}, \quad (13)$$

$$g_{21}(\mathbf{r}, \mathbf{r}', \omega_n) = \sum_{\alpha} \frac{v_{\alpha}(\mathbf{r}) u_{\alpha}^*(\mathbf{r}')}{i\omega_n - E_{\alpha}}, \quad (14)$$

$$g_{22}(\mathbf{r}, \mathbf{r}', \omega_n) = \sum_{\alpha} \frac{v_{\alpha}(\mathbf{r}) v_{\alpha}^*(\mathbf{r}')}{i\omega_n - E_{\alpha}}. \quad (15)$$

The LDOS is evaluated by using the thermal Green's functions as

$$N_{\uparrow}(E, \mathbf{r}) = -\frac{1}{\pi} \text{Im} g_{11}(\mathbf{r}, \mathbf{r}, i\omega_n \rightarrow E + i\eta) \quad (16)$$

for the up-spin electron contribution, and

$$N_{\downarrow}(E, \mathbf{r}) = \frac{1}{\pi} \text{Im} g_{22}(\mathbf{r}, \mathbf{r}, -i\omega_n \rightarrow E + i\eta) \quad (17)$$

for the down-spin electron contribution. Then, the total LDOS is given by

$$\begin{aligned} N(E, \mathbf{r}) &= N_{\uparrow}(E, \mathbf{r}) + N_{\downarrow}(E, \mathbf{r}) \\ &= \sum_{\alpha} \{ |u_{\alpha}(\mathbf{r})|^2 \delta(E - E_{\alpha}) + |v_{\alpha}(\mathbf{r})|^2 \delta(E + E_{\alpha}) \}. \end{aligned} \quad (18)$$

When we consider the differential tunnel conductance of STM experiments, the  $\delta$ -functions in eq. (18) are replaced by the derivative  $-f'(E)$  of the Fermi distribution function  $f(E)$ :  $N(E, \mathbf{r}) = -\sum_{\alpha} [|u_{\alpha}(\mathbf{r})|^2 f'(E_{\alpha} - E) + |v_{\alpha}(\mathbf{r})|^2 f'(E_{\alpha} + E)]$ .

By calculating the spin-spin correlation function  $\chi_{+,-}(\mathbf{r}, \mathbf{r}', i\Omega_n)$  from the Green's functions in Eqs. (12)-(15), we obtain the nuclear spin relaxation rate,<sup>33</sup>

$$\begin{aligned} R(\mathbf{r}, \mathbf{r}') &= \text{Im} \chi_{+,-}(\mathbf{r}, \mathbf{r}', i\Omega_n \rightarrow \Omega + i\eta) / (\Omega/T) |_{\Omega \rightarrow 0} \\ &= -\sum_{\alpha, \alpha'} [u_{\alpha}(\mathbf{r}) u_{\alpha'}^*(\mathbf{r}') v_{\alpha'}^*(\mathbf{r}) v_{\alpha}^*(\mathbf{r}')] \\ &\quad \times \pi T f'(E_{\alpha}) \delta(E_{\alpha} - E_{\alpha'}). \end{aligned} \quad (19)$$

We consider the case  $\mathbf{r} = \mathbf{r}'$  by assuming that the nuclear relaxation occurs at a local site. Then,  $\mathbf{r}$ -dependent relaxation time is given by  $T_1(\mathbf{r}) = 1/R(\mathbf{r}, \mathbf{r})$ . We use  $\delta(x) = \pi^{-1} \text{Im}(x - i\eta)^{-1}$  to handle the discrete energy level of the finite size calculation. We typically use  $\eta = 0.01t$ . In Eq. (19), the first term is proportional to  $N_{\uparrow}(\mathbf{r}, E) \times N_{\downarrow}(\mathbf{r}, E)$  when  $\mathbf{r} = \mathbf{r}'$ .

We typically consider the case of a unit cell with  $24 \times 24$  sites, where two vortices are accommodated. The vortex cores are located at  $(i_x, i_y) = (1, 1)$  and  $(N_r/2+1, N_r/2+1)$ . The spatially averaged hole density is set to  $n_h = 1 - \bar{n}_i \sim \frac{1}{8}$  by tuning the chemical potential  $\mu$ . By introducing the quasimomentum of the magnetic Bloch state, we obtain the wave function under the periodic boundary condition whose region covers many unit cells. In this paper, temperature  $T$  is scaled by  $T_c$  which is the superconducting critical temperature when  $U/t = 0$ .

For the initial state of our calculation, we give a lowest Landau level function of the vortex state for  $\Delta$ , and very weak incommensurate spin modulation for  $n_{\sigma}$  with the ordering vector  $\mathbf{Q} = (\pi, 2\pi(\frac{1}{2} - \epsilon))$  and  $\epsilon = \frac{1}{8}$  appropriate to the hole filling  $\frac{1}{8}$ . By iterating the calculation,  $M(\mathbf{r}_i) \rightarrow 0$  when the AFM is absent. When the AFM appears,  $M(\mathbf{r}_i)$  grows and makes checkerboard or stripe pattern depending on the parameters.

### III. PROPERTIES OF ANTIFERROMAGNETISM AROUND THE VORTEX CORE

We solve the BdG equation self-consistently with the on-site repulsive interaction  $U$ , using an eight-site peri-

odic vertical stripe state as an initial state. We consider the case that spin and charge modulations appear around the vortex core, which is stabilized by  $U$ . Then the self-consistent solution of the AFM-induced  $d$ -wave vortex is analyzed and compared with the “normal”  $d$ -wave vortex for  $U = 0$ .<sup>32,33</sup>

### A. Induced moment around the core

Figure 1 shows the spatial structure of vortex state, i.e., the amplitude of the  $d$ -wave order parameter  $|\Delta_d(\mathbf{r}_i)|$ , the staggered magnetization  $M(\mathbf{r}_i)$ , the charge density  $n(\mathbf{r}_i)$ , the zero-energy LDOS  $N(E = 0, \mathbf{r}_i)$ , within a unit cell for various  $U$ 's.

First, we consider the induced magnetic moment around the vortex core. In  $d$ -wave vortex case without AFM at  $U = 0$ , the superconductivity  $|\Delta_d(\mathbf{r})|$  is suppressed at the vortex core and the zero-energy LDOS has peak there (Fig. 1(a)). Using these low energy states, the staggered moment is induced centered at the vortex core for larger  $U$  case. It is seen from Fig. 1 that (1) At  $U = 0$  no moment appears. (2) The induced moment appears centered around the core at  $U > U_{\text{cr}}$ , and the moment grows as  $U$  increases. (3) The spatial structure of the induced moment changes from a simple AFM type to a stripe type when  $U > 3.1t$ . In the former simple AFM state has also checkerboard type modulation. This checkerboard modulation is barely seen in Fig. 1(c), where the “floor” in  $M(\mathbf{r})$  is modulated with eight-site period. (4) In the stripe case (Fig. 1(d)) the amplitude maximum of  $M(\mathbf{r})$  coincides with the vortex core in this example. These tendencies are already seen in our previous paper for the vortex state in the stripe state.<sup>30</sup>

In Fig. 2(a), we show the AFM moment at the core  $M_v$  as a function of  $U$  for the two cases  $V/t = -1$  and  $V/t = -2$ . The induced moment appears above the critical  $U_{\text{cr}}$ , which depends on  $V$ . The critical strength  $U_{\text{cr}}$  is larger for stronger pairing interaction  $V$ , as is seen from Fig. 2(a), because superconductivity tends to suppress the AFM moment. When  $U < U_{\text{cr}}$ ,  $M_v = 0$  and the vortex structure is the same as  $U = 0$  case. We show the  $T$ -dependence of  $M_v$  for several  $U$  values in Fig. 2(b). For  $U/t = 3.4$  the moment appears above  $T_c$ . In this strong  $U$  case, the spatial structure of the moment is a stripe type (see Fig. 1(d)), and at  $T > 0.5T_c$ , the stripe periodicity changes from eight site period by the temperature effect. For smaller  $U$ ,  $M(\mathbf{r})$  becomes a checkerboard type as shown in Fig. 1(c), and  $M_v$  appears at  $T_M$  below  $T_c$ . With decreasing  $U$ ,  $T_M$  decreases.

### B. Charge density around the core

The spatial variation of the charge density  $n(\mathbf{r})$  around the vortex core is shown also in Fig. 1, which is also affected by the induced AFM. While  $n(\mathbf{r})$  is suppressed at the vortex core at  $U = 0$ ,<sup>36</sup>  $n(\mathbf{r})$  increases with ap-

proaching the core, when  $M_v$  appears at  $U > U_{\text{cr}}$ . These properties of the charge structure are related to the modulation of the LDOS, as discussed later. In the large  $U$  case giving  $T_M > T_c$ , the stripe structure becomes eminent and the charge stripe structure is seen in Fig. 1(d). When comparing with the spin stripe structure of  $M(\mathbf{r})$ ,  $n(\mathbf{r})$  has minimum at the node of the  $M(\mathbf{r})$  oscillation, implying that the excess hole carriers accumulate there. The periodicity of the charge modulation is four-site, in our doping level  $n_h \sim 1/8$ . It is half of the spin structure periodicity.

The  $U$ -dependence of the charge at the core  $n_v$  is shown in Fig. 2(c), where we see that the suppressed  $n_v$  at  $U < U_{\text{cr}}$  is increased with the growth of  $M_v$  when  $U > U_{\text{cr}}$ . The  $T$ -dependence of  $n_v$  is shown in Fig. 2(d). When  $U = 0$ ,  $n_v$  is reduced around the vortex core at low temperature because of the particle-hole asymmetry.<sup>36</sup> For  $U > U_{\text{cr}}$ , the decreasing dependence of  $n_v$  on lowering temperature changes to the increasing one at  $T < T_M$  where the moment begins to appear. These charge behavior is similar to the case when commensurate AFM is induced around the vortex core.<sup>25,26</sup>

### C. Fourier component of the spin and charge modulation

In order to see the checkerboard modulation of  $M(\mathbf{r})$  superimposed in the basic AFM variation, we calculate the Fourier transformation  $S_{z,\mathbf{q}}$  and  $n_{\mathbf{q}}$  from  $S_z(\mathbf{r}_i)$  and  $n(\mathbf{r}_i)$ , respectively. In addition to the peak of the vortex lattice period,  $S_{z,\mathbf{q}}$  has the peaks at  $\mathbf{q} = \mathbf{Q}_1 = (\frac{3}{4}\pi, \pi)$  and/or  $\mathbf{q} = \mathbf{Q}_2 = (\pi, \frac{3}{4}\pi)$ , where we set the lattice constant to be unity. These  $\mathbf{Q}_1$  and  $\mathbf{Q}_2$  are, respectively, ordering vectors of the eight-site period spin structure along  $x$  and  $y$  directions. These peaks correspond to the neutron scattering peaks observed in LSCO.<sup>7,8,9</sup> As for the charge structure,  $\mathbf{q}$  has the peaks at  $\mathbf{q} = 2\mathbf{Q}_1$  and/or  $\mathbf{q} = 2\mathbf{Q}_2$ . In Fig. 3(a), we show the  $U$ -dependence of the peak height for  $S_{z,\mathbf{q}}$  at  $\mathbf{q} = \mathbf{Q}_1$  and  $\mathbf{q} = \mathbf{Q}_2$ . When  $U < 3.1t$ , the peak heights at  $\mathbf{Q}_1$  and at  $\mathbf{Q}_2$  are the same, meaning the checkerboard modulation both  $x$  and  $y$  directions. Since the peak height increases, the spin modulation becomes eminent with increasing  $U$ . When  $U$  becomes larger than  $3.1t$ , one of the peaks for  $S_{z,\mathbf{q}}$  vanishes, and one of the peaks remains at  $\mathbf{Q}_1$  or  $\mathbf{Q}_2$ , which means a one-dimensional stripe, as is seen in Fig. 1(d).

This checkerboard-stripe transition is also seen in the Fourier transformation of the charge structure shown in Fig. 3(b). At  $U < 3.1t$ ,  $n_{\mathbf{q}}$  has the peaks both at  $2\mathbf{Q}_1$  and  $2\mathbf{Q}_2$ , meaning four site periodic checkerboard charge structure. At  $U \geq 3.1t$ ,  $n_{\mathbf{q}}$  has the peak either at  $2\mathbf{Q}_1$  or at  $2\mathbf{Q}_2$ , meaning four site periodic stripe structure.

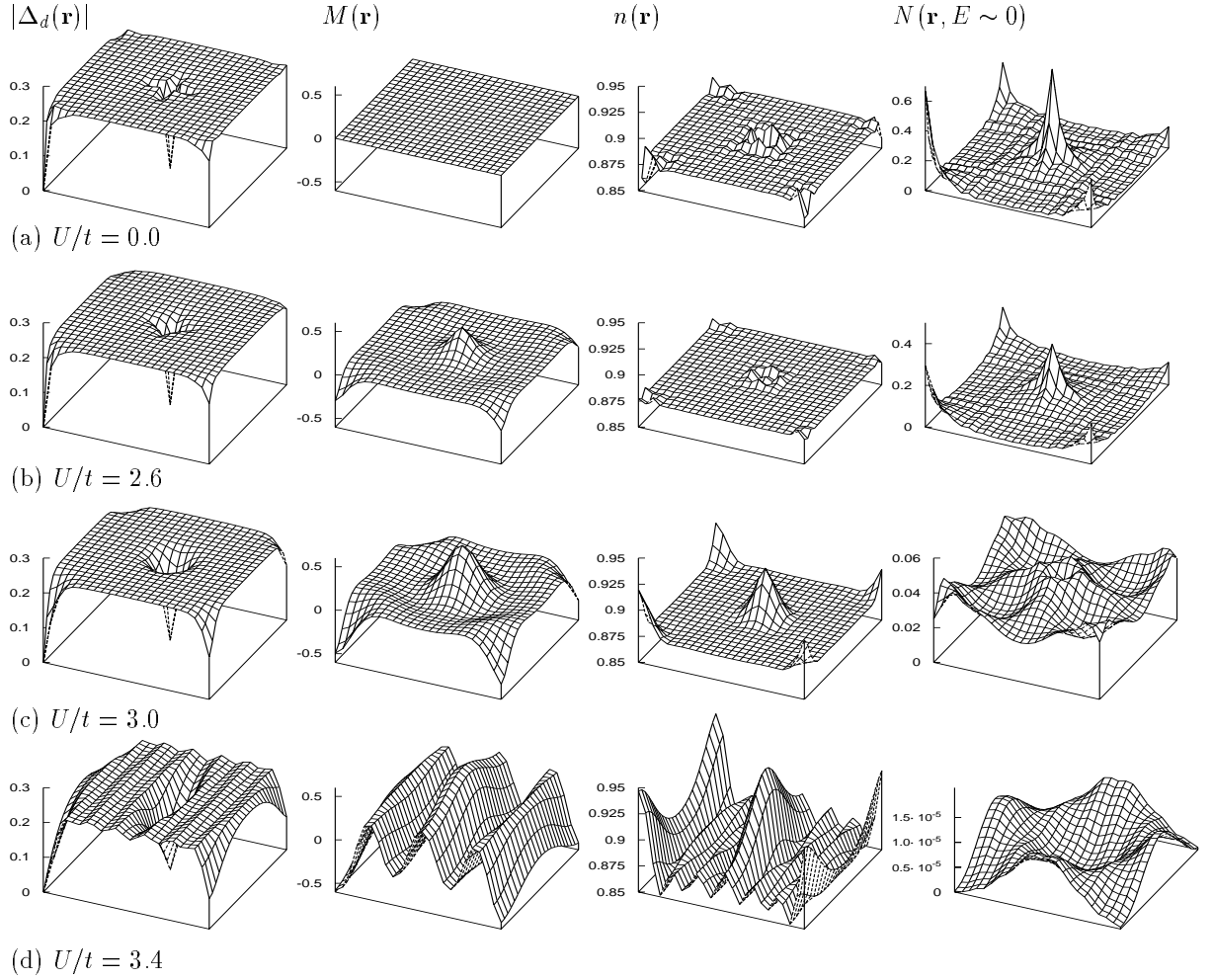


FIG. 1: Spatial variation of the vortex state at  $T = T_c/40$  for  $U/t=0.0$  (a), 2.6 (b), 3.0 (c) and 3.4 (d). From left to right, we show the amplitude of the  $d$ -wave order parameter  $|\Delta_d(\mathbf{r})|$ , the staggered magnetization  $M(\mathbf{r}_i)$ , the charge density  $n(\mathbf{r}_i)$ , and the zero-energy LDOS  $N(E = 0, \mathbf{r}_i)$  within a unit cell. The vortex center is located at the center  $(i_x, i_y) = (N_r/2 + 1, N_r/2 + 1)$  and a corner(1,1).

#### D. Vortex core radius

Here, we discuss the vortex core shape and radius from the spatial structure of  $|\Delta_d(\mathbf{r})|$ . As seen from  $|\Delta_d(\mathbf{r})|$  in Fig. 1(a), when the AFM is absent at  $U < U_{cr}$ , we see the fourfold symmetric vortex core shape, reflecting the fourfold symmetry of the  $d_{x^2-y^2}$ -wave pairing potential in the momentum space.<sup>1</sup> After the AFM appears at  $U > U_{cr}$ , the vortex core becomes circular shape, as shown in Fig. 1(c). In the stripe case at  $U/t = 3.4$ ,  $|\Delta_d(\mathbf{r})|$  also shows four-site periodic structure, where  $|\Delta_d(\mathbf{r})|$  is enhanced at the hole-rich site. In this case, vortex core shape is enlarged along the stripe direction.

To discuss the core radius, in Fig. 4 we show the profile of the order parameter  $|\Delta_d(\mathbf{r}_i)|$  and staggered magnetization  $M(\mathbf{r}_i)$  along the  $x$ -direction, which is the next NN vortex direction and also the parallel direction to the stripe. When the magnetization appears around the core, the  $d$ -wave order parameter is suppressed, therefore the

radius of the vortex core becomes large. To estimate the core radius, we fit the profile of  $|\Delta_d(\mathbf{r}_i)|$  along the next NN vortex direction by  $\Delta_M \tanh^A(r/B)$ , where  $\Delta_M$  is the amplitude in the bulk, and  $A$  and  $B$  are fitting parameters. Our definition of the core radius  $R$  is the radius where the fitting line is recovered to  $\Delta_M/C = 0.6\Delta_M$ . Thus,  $R$  is given by  $R = B \ln \sqrt{(C^{1/A} + 1)/(C^{1/A} - 1)}$ .

We show the temperature dependence of the core radius in Fig. 5. When  $U = 0$ , the core radius  $R$  monotonically shrinks as  $T$  lowers, according to the Kramer-Pesch (KP) effect<sup>37</sup> and saturates at lower  $T$  because of the quantum limit behavior<sup>38</sup> even in the  $d$ -wave superconductor. For finite  $U(> U_{cr})$  cases shown in Fig. 5, the deviation from the KP linear curve occurs below the temperature  $T_M$  where  $M_v$  appears (see Fig. 2(b)). That is, the shrinkage of  $R$  stops at  $T_M$ , and the core radius increases as  $T$  lowers. This is caused by the growth of the moment induced around the core which destroys the condensation locally, enlarging  $R$ . This feature coincides

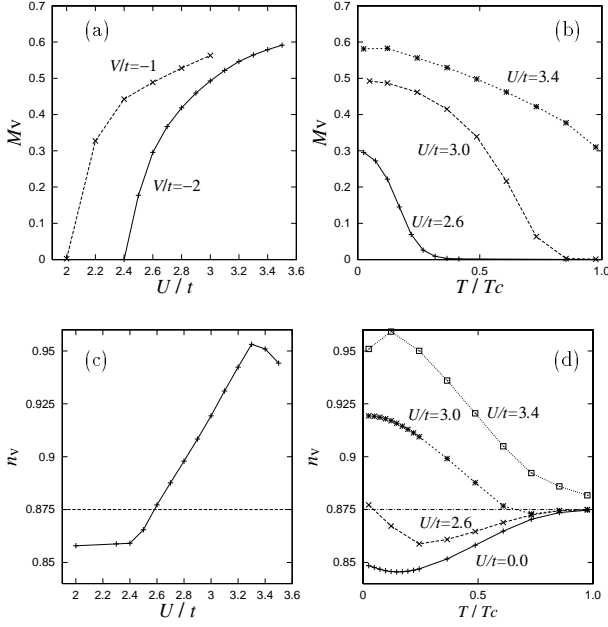


FIG. 2: The AFM moment  $M_v$  and the charge density  $n_v$  at the vortex center. (a)  $U$ -dependence of  $M_v$  at  $T = T_c/40$  for  $V/t = -1$  and  $-2$ . (b)  $T$ -dependence of  $M_v$  for  $U/t = 0, 2.6, 3.0$  and  $3.4$ . (c)  $U$ -dependence of  $n_v$  at  $T = T_c/40$  for  $V/t = -2$ . (d)  $T$ -dependence of  $n_v$  for  $U/t = 0, 2.6, 3.0$  and  $3.4$ .

with the  $\mu$ SR experiment on  $\text{La}_{2-x}\text{Sr}_x\text{CuO}_4$  by Kadono *et al.*,<sup>11</sup> where as  $x$  decreases the  $R$  stops at higher  $T$  and becomes larger. If we interpret the doping dependence in terms of the  $U$ -change, the smaller  $x$  should correspond to the larger  $U$ . This correspondence is natural because as going into underdopings the stripe tendency is strengthened. Tsuchiura *et al.*,<sup>21,41</sup> assert that the core radius becomes smaller as approaching to half-filling in their t-J model calculation, it contradicts  $\mu$ SR experimental results and our extended Hubbard model calculation.

The order parameter  $\Delta_d$  vanishes at the vortex core and recovers to the bulk value continuously. The spatial variation of the  $\Delta_d$  induces the order parameters with other symmetry, such as an extended  $s$ -wave or  $p_x \pm ip_y$ -wave components, around the core.<sup>31</sup> Here, we only discuss the  $d$ -wave triplet pairing component. As increasing the repulsive interaction  $U$ , the magnetization arises around the vortex core as mentioned before. In the range of  $U > U_c$ , the checkerboard pattern appears on the floor. And in  $U/t > 3.1$ , the stripe structure which is modulated by vortices appears. In these cases, small triplet- $d$ -wave component  $\Delta_d^{\text{triplet}}$  appears around the core.<sup>31,40</sup> Figure 4 shows the profile of  $|\Delta_d^{\text{triplet}}(\mathbf{r}_i)|$ . By increasing  $U$ , the maximum point in  $|\Delta_d^{\text{triplet}}|$  moves to outside the core and the amplitudes become large.

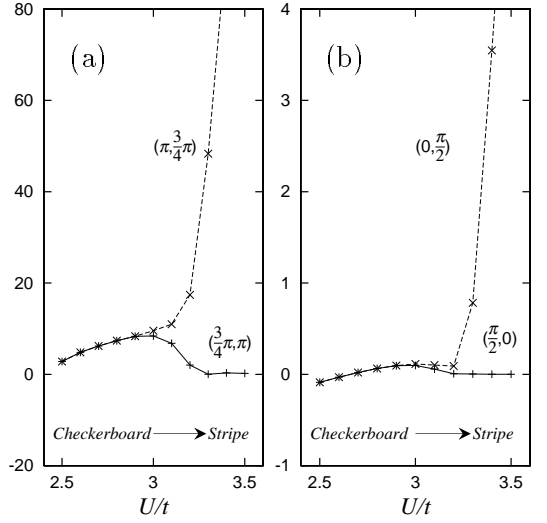


FIG. 3:  $U$ -dependence of the Fourier component. (a) Eight-site periodic Fourier component of the magnetization,  $S_{z,\mathbf{Q}}$  for  $\mathbf{Q} = (\frac{3}{4}\pi, \pi)$  and  $\mathbf{Q} = (\pi, \frac{3}{4}\pi)$ . (b) Four-site periodic Fourier component of the charge density,  $n_{2\mathbf{Q}}$  for  $2\mathbf{Q} = (\frac{1}{2}\pi, 0)$  and  $2\mathbf{Q} = (0, \frac{1}{2}\pi)$ .  $T = T_c/40$ .

#### IV. LOCAL DENSITY OF STATES

We study the effect of the induced AFM in the LDOS. Figure 6(a) shows the LDOS at the vortex core site. For  $U = 0$  in the upper panel, we see the ZEP at  $E \sim 0$ , which is a typical feature of the vortex in  $d$ -wave superconductors.<sup>2</sup> The small suppression at  $E \sim 0$  may come from the induced other component, such as an extended  $s$ -wave, around the vortex core.<sup>42</sup> However, this effect is small. The charge density for each spin is given by

$$\begin{aligned} n_{i,\uparrow} &= \int dE N_{\uparrow}(E, \mathbf{r}_i) f(E), \\ n_{i,\downarrow} &= \int dE N_{\downarrow}(E, \mathbf{r}_i) f(E). \end{aligned} \quad (20)$$

When we see the spectrum inside the superconducting gap at  $U = 0$ , the weight of  $N(E, \mathbf{r})$  for  $E < 0$  is smaller than that for  $E > 0$ , reflecting the suppression of  $n(\mathbf{r}_i)$  around the core shown in Fig. 1(a).

When the AFM appears at  $U > U_{\text{cr}}$ , the ZEP is suppressed around  $E = 0$ . With increasing  $U$ , the suppression becomes eminent, and the peaks are shifted to larger  $|E|$ , as shown in the middle and lower panels in Fig. 6(a). When  $M(\mathbf{r}_i) \neq 0$ ,  $N_{\uparrow}(E, \mathbf{r}_i) \neq N_{\downarrow}(E, \mathbf{r}_i)$ . Since  $n_{\uparrow,i} < n_{\downarrow,i}$  in the case  $S_z(\mathbf{r}_i) < 0$  at the site of the vortex center,  $N_{\uparrow}(E, \mathbf{r}_i) < N_{\downarrow}(E, \mathbf{r}_i)$  for  $E < 0$  and  $N_{\uparrow}(E, \mathbf{r}_i) > N_{\downarrow}(E, \mathbf{r}_i)$  for  $E > 0$ , following the relation in Eq. (20). Therefore, split peaks at positive and negative energy, respectively, come from the up-spin and down-spin contribution. After the AFM appears, the weight of the LDOS for  $E > 0$  shifts to that for  $E < 0$ , reflecting

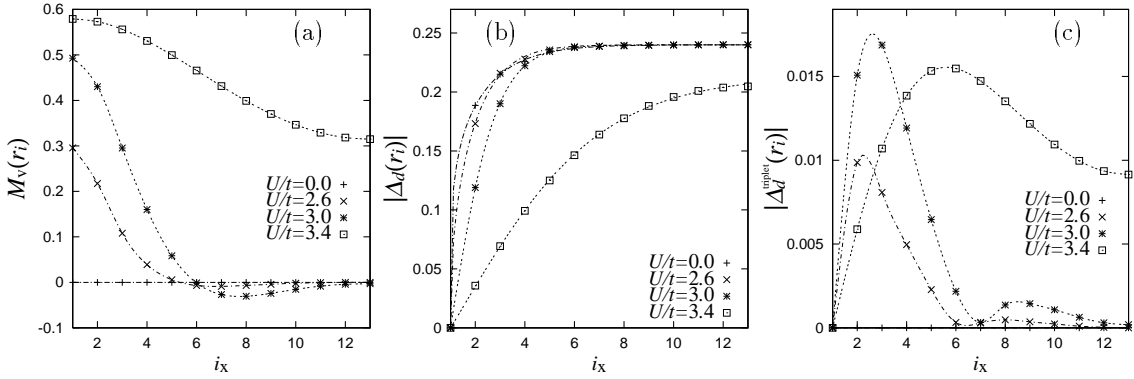


FIG. 4: The profile of the staggered magnetization  $M(\mathbf{r})$  (a), the  $d$ -wave singlet order parameter amplitude  $|\Delta_d(\mathbf{r}_i)|$  (b), and the  $d$ -wave triplet order parameter amplitude  $|\Delta_d^{\text{triplet}}(\mathbf{r}_i)|$  (c) along the  $x$  axis direction,  $i_y = 1$ . The vortex core is located at  $i_x = 1$ .  $T = T_c/40$ .  $U/t = 0, 2.6, 3.0$  and  $3.4$ .

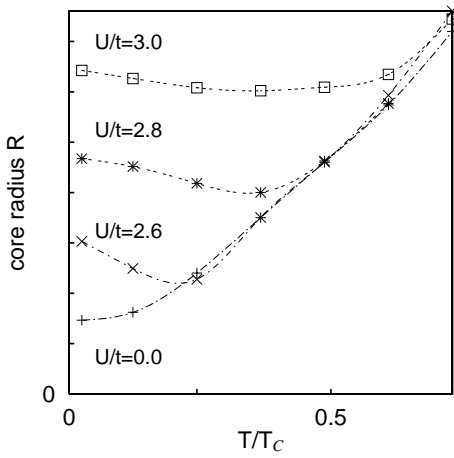


FIG. 5: Temperature dependence of the core radius  $R$  for  $U = 0, 2.6, 2.8$  and  $3.0$ . The departure from the monotonic decreasing curve of  $U = 0.0$  occurs at the corresponding  $T_M$ .

the enhancement of  $n(\mathbf{r}_i)$  around the core shown in Figs. 1(c) and 1(d).

In Fig. 6(b), we show the LDOS at the site next to the vortex center site. There, while the ZEP is smeared at  $U = 0$ , the suppression of the LDOS around  $E = 0$  is seen as in the vortex center site. Since this site has up-spin moment, split peaks at positive and negative energy, respectively, comes from the down-spin and up-spin contribution. The LDOS at farthest site in the midpoint between next NN vortices is shown in Fig. 6(c), which has spectrum as in the uniform  $d$ -wave superconductor at zero field. By the induced AFM, the low energy state is slightly suppressed.

The spatial structure of the LDOS at  $E \sim 0$  is also displayed in Fig. 1. The ZEP height at the vortex core becomes low as the moment  $M_v$  grows. In Figs. 1(c) and 1(d) where the induced moment  $M_v$  is rather large, the peak structure at the core is removed completely and the LDOS at the core is small compared with its surroundings, giving rise to a “caldera” type landscape. This is an

origin of the so-called “empty” core observed by STM,<sup>15</sup> as discussed later.

## V. NUCLEAR MAGNETIC RELAXATION TIME AND THE RESONANCE LINE SHAPE

As mentioned in the introduction, NMR is a powerful method to simultaneously know the field distribution in vortex lattice through the resonance pattern (Redfield pattern) and the spatial profile of the zero-energy quasi-particles through the relaxation time  $T_1$ . In this section we calculate the site-selective  $T_1$  based on the solutions obtained in the previous sections and examine the outcomes from the “anomalous”  $d$ -wave vortex core.

In Fig. 7, we plot the  $T$ -dependence of the  $1/(T_1T)$ . Far from the vortex core (line denoted as “bulk site” in the figure),  $T_1$  shows the conventional  $T_1^{-1} \sim T^3$  behavior of the line node case as in the bulk at zero field. As shown in Fig. 7(a),  $1/(T_1T)$  shows peak below  $T_c$  at the core site. And, when  $U/t = 0$ ,  $1/(T_1T)$  is increased on lowering  $T$  due the presence of ZEP. When  $M_v$  appears at  $T_M (< T_c)$ , as shown in Fig. 2(b),  $1/(T_1T)$  behavior deviates from the line of the  $U = 0$  case at  $T_M$ . Below  $T_M$ ,  $1/(T_1T)$  is suppressed with lowering  $T$ , reflecting the decrease of the zero-energy DOS by the splitting of ZEP in Fig. 6(a). Therefore, we see that, on lowering  $T$ ,  $1/(T_1T)$  increases at  $T > T_M$  and decreases at  $T < T_M$  at the vortex core site, which is consistent with the observed  $1/(T_1T)$  behavior.<sup>27</sup> At NN-site (Fig. 7(b)),  $1/(T_1T)$  is also suppressed at  $T < T_M$  by losing DOS for  $E \sim 0$ .

Next, we study the internal field dependence of  $1/(T_1T)$ . The  $1/(T_1T)$  can be distinguished spatially by its resonant frequency in NMR experiment. The frequency depends on the internal magnetic field  $H_{\text{int}}(\mathbf{r})$ , which consists of a contribution from the screening current in the vortex lattice and the direct contribution from the AFM-moment. At first, we evaluate  $H_{\text{int}}^j(\mathbf{r})$  from the contribution via the screening current distribution

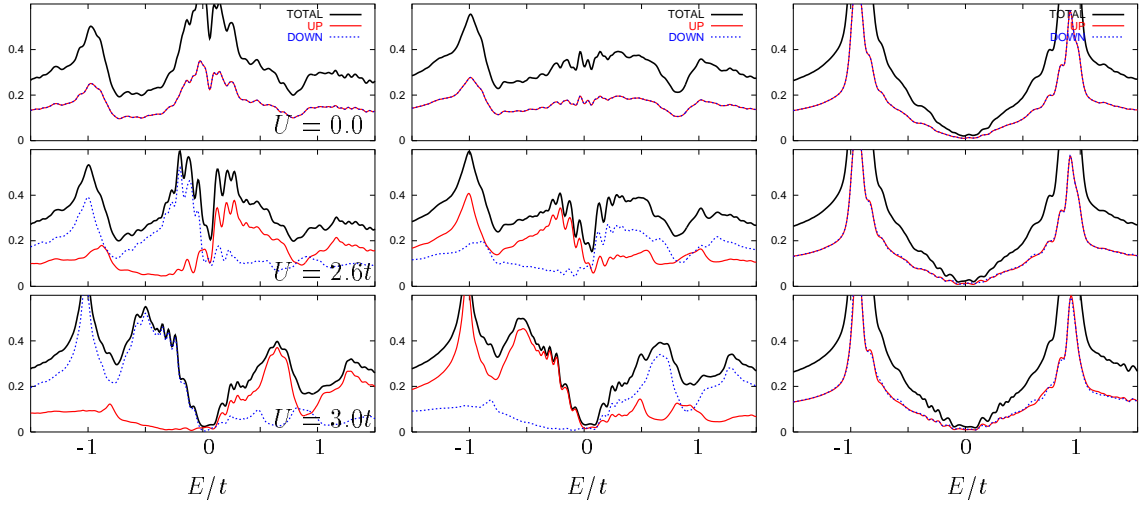


FIG. 6: The local density of states  $N(E, \mathbf{r}_i)$  for  $U/t = 0.0, 2.6, 3.0$  at  $T = T_c/40$ . (a) Vortex center site (1,1), (b) Nearest neighbor site (1,2) to the vortex center, (c) Bulk site (1,12) in the midpoint between next NN vortices. We also show the up- and down-spin contributions,  $N_\uparrow(E, \mathbf{r}_i)$  and  $N_\downarrow(E, \mathbf{r}_i)$ . The energy is scaled by  $t$ .

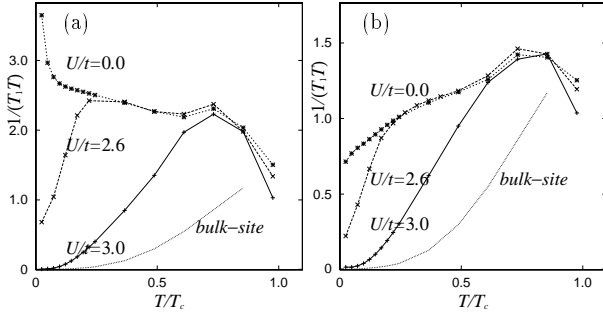


FIG. 7: Temperature dependence of  $1/(T_1 T)$  for  $U/t = 0, 2.6$  and  $3.0$ . (a) Vortex center site (1,1), (b) NN-site (1,2) next to the center. The  $1/(T_1 T)$  is normalized by the value at  $T_c$ . The line denoted as “bulk site” shows  $1/(T_1 T)$  at the furthest site from the vortex in the midpoint between next NN vortices.  $T_M/T_c \sim 0.25$  ( $U/t = 2.6$ ) and  $0.75$  ( $U/t = 3.0$ )

through the Maxwell equation:

$$\nabla \times \mathbf{H} = \frac{4\pi}{c} \mathbf{j}(\mathbf{r}). \quad (21)$$

The current is calculated as

$$j_{\hat{e}}(\mathbf{r}_i) = 2|e|c \text{Im} \{ \tilde{t}_{i+\hat{e},i} \sum_{\sigma} \langle a_{i+\hat{e},\sigma}^\dagger a_{i,\sigma} \rangle \} \quad (22)$$

$$= 2|e|c \text{Im} \{ \tilde{t}_{i+\hat{e},i} \sum_{\alpha} [u_{\alpha}^*(\mathbf{r}_{i+\hat{e}}) u_{\alpha}(\mathbf{r}_i) f(E_{\alpha}) + v_{\alpha}(\mathbf{r}_{i+\hat{e}}) v_{\alpha}^*(\mathbf{r}_i) (1 - f(E_{\alpha}))] \} \quad (23)$$

for the  $\hat{e}$ -direction bond ( $\hat{e} = \pm \hat{x}, \pm \hat{y}$ ) at the site  $\mathbf{r}_i$ . The screening current  $j_{\hat{e}}(\mathbf{r}_i)$  circles around each vortex core. When  $M_v \neq 0$ ,  $j_{\hat{e}}(\mathbf{r}_i)$  exhibits the staggered-like fluctuation current.<sup>20</sup> It does not appear when  $M_v = 0$  even if  $U/t > 0$ .

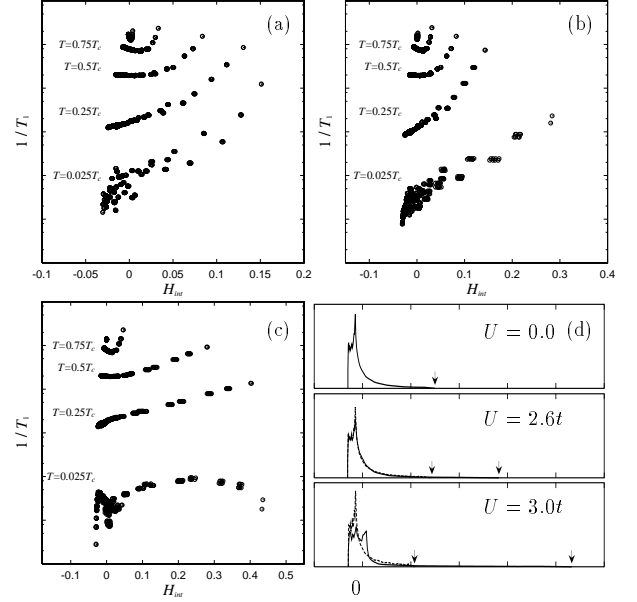


FIG. 8: The distribution of  $1/T_1$  as a function of the internal magnetic field  $H_{\text{int}}$  at  $T/T_c = 0.025, 0.25, 0.5, 0.75$  and  $0.95$  in the case  $U/t = 0.0$  (a),  $2.6$  (b), and  $3.0$  (c). Vertical axis is in log-scale, and horizontal axis is in arbitrary unit. The internal field distribution function (d) (resonance line shape of NMR) at  $T/T_c = 0.025$  for  $H_{\text{int}}(\mathbf{r})$  (solid lines) and  $H_{\text{int}}^j(\mathbf{r})$  (dashed lines). The right side (left side) arrow shows the maximum of  $H_{\text{int}}$  ( $H_{\text{int}}^j$ ).

Figure 8 shows  $1/T_1$  as a function of the internal field  $H_{\text{int}}$  for some temperatures. Here, we take account of the contribution from the AFM-moment. The internal field



is given by

$$H_{\text{int}}(\mathbf{r}) = \sqrt{(H_{\text{int}}^j(\mathbf{r}) + H_0)^2 + m^2 M^2(\mathbf{r})} - H_0 \\ \simeq H_{\text{int}}^j(\mathbf{r}) + \frac{m^2}{2H_0} M^2(\mathbf{r}) \quad (24)$$

for  $H_{\text{int}}^j(\mathbf{r}), |mM(\mathbf{r})| \ll H_0$ .  $H_0$  is the external field.  $H_{\text{int}}^j(\mathbf{r})$  is a contribution of the screening current  $j_{\hat{e}}$  in the vortex lattice. The  $mM(\mathbf{r})$  with a numerical factor  $m$  is the direct contribution from AFM moment. Here, we assume that the magnetic moments are parallel to the CuO-layer as in the AF-state at the half-filling. And we choose  $m$  to reproduce the observed line shape of NMR.<sup>43</sup>

The internal field distribution function, corresponding to the resonance line shape of NMR, is shown for lowest temperature case in Figs. 8(a)-(c). The horizontal width of  $1/T_1$ -distribution corresponds to the width of the resonance line shape for higher temperature data. As increasing temperature, the width of the resonance line shape becomes narrow (Fig. 8(a)) since the internal field narrowly distributes in the vortex lattice. The width depends on the radius of the core. As the core radius becomes larger, the maximum point of the screening current becomes far from the vortex center, and the peak of the internal field at the vortex center becomes broad. Thus, the width of the resonance line shape becomes narrow.

This relation between the width of the resonant line shape and the vortex core radius appears also in the  $U$ -dependence, if we neglect the contribution from  $M(\mathbf{r})$ . We compare the field distribution function of  $H_{\text{int}}^j(\mathbf{r})$  at  $U/t = 0, 2.6$  and  $3.0$ , which are shown by dashed lines in Fig. 8(d). In this figure left side arrows show the maximum of  $H_{\text{int}}^j(\mathbf{r})$ . In the case  $U/t = 2.6$  and  $3.0$  where the moment appears around the core at low temperatures, the core radius  $R$  is larger, and the width of the line shape becomes narrower at low temperature.

The realistic line shape observed in NMR includes the contribution of the AFM moment. The solid lines in Fig. 8(d) show the field distribution function of  $H_{\text{int}}(\mathbf{r})$  given by Eq. 24. In this figure, right side arrows show the maximum of  $H_{\text{int}}(\mathbf{r})$ . In the case  $U/t = 2.6$  and  $3.0$ , by the AFM effect, the resonance line shape becomes broader and have a long tail toward the higher- $H_{\text{int}}$  side. After the magnetization appears, the ZEP in the LDOS splits and  $1/T_1$  becomes small. When we see the  $1/T_1$ -behavior as a function of  $H_{\text{int}}$ , as in Fig. 8,  $1/T_1$  shows the same behavior as the  $U = 0$  case for  $T > T_M$ . At  $T < T_M$ , the effective internal field is shifted toward higher- $H_{\text{int}}$  side, and  $1/T_1$  is decreased. These AFM contributions are eminent at higher- $H_{\text{int}}$  region, where signals come from the spatial region around the vortex core. In Fig. 8(c), as  $H_{\text{int}}$  increases,  $1/T_1$  decreases near the vortex core region (high  $H_{\text{int}}$  region) at low temperature, reflecting the special feature of the spatial structure, namely “caldera” structure of  $N(E = 0, \mathbf{r})$  shown in Fig. 1(c). This special feature is observed by Kakuyanagi *et al.*<sup>43</sup> The spa-

tial structure of this  $1/T_1(\mathbf{r})$ -behavior appears at lowest temperature when  $U$  is strong (near the stripe state). To reproduce the suppression of  $1/T_1$  at the vortex core region, the choice of the Fermi surface shape (i.e.  $t'$  and  $t''$ ) is important. For example, we cannot obtain “caldera” type-LDOS structure when  $t' = 0$ .

## VI. CONCLUSION AND DISCUSSION

In this paper, based on the extended Hubbard Hamiltonian, we have studied the vortex structure when the incommensurate AFM is induced around the vortex core by the competition between AFM and superconductivity due to the on-site repulsive interaction  $U$ . We calculate the spatial distribution of the  $d$ -wave superconducting order parameter, the magnetization, charge density, the local density of states and the nuclear spin relaxation rate  $T_1$ , and clarify the  $U$ - and temperature-dependences.

As increasing  $U$ , the AFM with weak checkerboard modulation appears around the vortex core at  $U > U_{\text{cr}}$ , where the AFM-moment appears at  $T_M (< T_c)$ . At further large  $U$ , the checkerboard modulation changes to the stripe modulation, where  $T_M > T_c$ . This transitions is clearly seen by analyzing the Fourier component corresponding the ordering vector of the incommensurate modulation.

By the induced AFM around the vortex core, the ZEP at the vortex core at  $U = 0$  splits, and the zero-energy density of states is suppressed. Reflecting this LDOS structure,  $1/T_1$  is suppressed at the vortex core in low temperature range. That is, on lowering  $T$ ,  $1/T_1$  is enhanced at  $T > T_M$  and decreased at  $T < T_M$ . These  $T_1$ -behaviors are consistent with the observation.<sup>27</sup> We also discuss the AFM effect on the internal field distribution, relating to the resonance line shape in NMR.

The spectrum structure of the LDOS is related to the spin and charge structure, such as the suppression (enhancement) of the charge density around the vortex core when the AFM is absent (present). The difference of the LDOS between up-spin and down-spin is essentially important especially to discuss the transport phenomena.

We also show that the vortex core radius becomes large as the AFM appears around the core. This behavior explains the doping dependence in recent  $\mu\text{SR}$  experiment. In this way, the induced AFM contribution plays an important role in the study of the various physical properties in the vortex state of high  $T_c$ -cuprate.

## Acknowledgments

We thank K. Kakuyanagi, K. Kumagai, Y. Matsuda, K. Ishida and V.F. Mitrović on their NMR for useful discussions. We thank R. Kadono on their  $\mu\text{SR}$  for useful discussions. We thank Y. Tanaka and M. Ogata, for useful discussions.

- 
- \* Electronic address: takigawa@mp.okayama-u.ac.jp;  
URL: <http://mp.okayama-u.ac.jp/~takigawa/>
- <sup>1</sup> M. Ichioka, N. Enomoto, N. Hayashi and K. Machida, Phys. Rev. B **53** 2233 (1996). M. Ichioka, N. Hayashi, N. Enomoto and K. Machida, Phys. Rev. B **53** 15316 (1996). M. Ichioka, N. Hayashi and K. Machida, Phys. Rev. B **55** 6565 (1997). N. Hayashi, M. Ichioka and K. Machida, Phys. Rev. B **56** 9052 (1997).
  - <sup>2</sup> M. Franz and Z. Tešanović, Phys. Rev. Lett. **80** 4763 (1998).
  - <sup>3</sup> M. Ichioka, A. Hasegawa and K. Machida, Phys. Rev. B **59** 8902 (1999) and 184 (1999).
  - <sup>4</sup> N. Schopohl and K. Maki, Phys. Rev. B **52** 490 (1995).
  - <sup>5</sup> Y. Wang, A.H. MacDonald, Phys. Rev. B **52** 3876 (1995).
  - <sup>6</sup> J.E. Hoffman, E.W. Hudson, K.M. Lang, V. Madhavan, H. Eisaki, S. Uchida and J.C. Davis, Science **295** 466 (2002).
  - <sup>7</sup> B. Lake, H.M. Rønnow, N.B. Christensen, G. Aeppli, K. Lefmann, D.F. McMorrow, P. Vorderwisch, P. Smeibidl, N. Mangkorntong, T. Sasagawa, M. Nohara, H. Takagi and T.E. Mason, Nature **415** 299 (2002).
  - <sup>8</sup> S. Katano, M. Sato, K. Yamada, T. Suzuki and T. Fukase, Phys. Rev. B **62** R14677 (2000).
  - <sup>9</sup> B. Khaykovich, Y.S. Lee, R. W. Erwin, S.-H. Lee, S. Wakimoto, K.J. Thomas, M.A. Kastner and R.J. Birgeneau, Phys. Rev. B **66** 014528 (2002).
  - <sup>10</sup> J.E. Sonier, K.F. Poon, G.M. Luke, P. Kyriakou, R.I. Miller, Ruixing Liang, C.R. Wiebe, P. Fournier and R.L. Greene, Phys. Rev. Lett. **91** 147002 (2003). R.I. Miller, R.F. Kiefl, J.H. Brewer, J.E. Sonier, J. Chakhalian, S. Dunsiger, G.D. Morris, A.N. Price, D.A. Bonn, W.H. Hardy and R. Liang, Phys. Rev. Lett. **88** 137002 (2002). J.E. Sonier, J.H. Brewer, R.F. Kiefl, R.I. Miller, G.D. Morris, C.E. Stronach, J.S. Gardner, S.R. Dunsiger, D.A. Bonn, W.N. Hardy, R. Liang and R.H. Heffner, Science **292** 1692 (2001).
  - <sup>11</sup> R. Kadono, W. Higemoto, A. Koda, M.I. Larkin, G.M. Luke, A.T. Savici, Y.J. Uemura, K.M. Kojima, T. Okamoto, T. Kakeshita, S. Uchida, T. Ito, K. Oda, M. Takigawa, M. Ichioka and K. Machida, preprint.
  - <sup>12</sup> V.F. Mitrović, E.E. Sigmund, M. Eschrig, H.N. Bachman, W.P. Halperin, A.P. Reyes, P. Kuhns and W.G. Moulton, Nature **413** 501 (2001).
  - <sup>13</sup> K. Kakuyanagi, K. Kumagai and Y. Matsuda, Phys. Rev. B **65** 60503 (2002).
  - <sup>14</sup> H.F. Hess, R.B. Robinson, R.C. Dynes, J.M. Valles, Jr. and J.V. Waszczak, Phys. Rev. Lett. **62** 214 (1989). H.F. Hess, R.B. Robinson and J.V. Waszczak, Phys. Rev. Lett. **64** 2711 (1990).
  - <sup>15</sup> Ch. Renner, B. Revaz, J.-Y. Genoud, K. Kadowaki and Ø. Fischer, Phys. Rev. Lett. **80** 149 (1998).
  - <sup>16</sup> D.P. Arovas, A.J. Berlinsky, C. Kallin and S.C. Zhang, Phys. Rev. Lett. **79** 2871 (1997).
  - <sup>17</sup> S.C. Zhang, Science **275** 1089 (1997).
  - <sup>18</sup> M. Franz, D. E. Sheehy and Z. Tešanović, Phys. Rev. Lett. **88** 257005 (2002). M. Franz and Z. Tešanović, Phys. Rev. B **63** 064516 (2001).
  - <sup>19</sup> M. Ogata, J. Mod. Phys. B **13** 3560 (1999).
  - <sup>20</sup> J. Kishine, P.A. Lee and X.G. Wen, Phys. Rev. Lett. **86** 5365 (2001) and Phys. Rev. B **65** 064526 (2002).
  - <sup>21</sup> H. Tsuchiura, M. Ogata, Y. Tanaka and S. Kashiwaya, Phys. Rev. B **68** 012509(2003).
  - <sup>22</sup> E. Demler, S. Sachdev and Y. Zhang, Phys. Rev. Lett. **87** 067202 (2001).
  - <sup>23</sup> J.-X. Zhu, I. Martin and A.R. Bishop, Phys. Rev. Lett. **89** 067003 (2002).
  - <sup>24</sup> M. Takigawa, M. Ichioka and K. Machida, Phys. Rev. Lett. **90** 047001 (2003).
  - <sup>25</sup> J.-X. Zhu and C.S. Ting, Phys. Rev. Lett. **87** 147002 (2001).
  - <sup>26</sup> Y. Chen, Z.D. Wang, C.S. Ting, Phys. Rev. B **67** 220501 (2003). Y. Chen, J.-X. Zhu and C.S. Ting, cond-mat/0302114. Y. Chen and C.S. Ting, Phys. Rev. B **65** 180513(R) (2002). Yan Chen, H.Y. Chen and C.S. Ting Phys. Rev. B **66** 104501 (2002). Y. Chen, Z.D. Wang, J.-X. Zhu and C.S. Ting, Phys. Rev. Lett. **89** 217001 (2002).
  - <sup>27</sup> K. Kakuyanagi, K. Kumagai, Y. Matsuda and M. Hasegawa, Phys. Rev. B **90** 197003 (2003).
  - <sup>28</sup> V.F. Mitrović, E.E. Sigmund, W.P. Halperin, A.P. Reyes, P. Kuhns and W.G. Moulton, Phys. Rev. B **67** 220503 (2003).
  - <sup>29</sup> K. Machida, Physica C **158** 192 (1989). M. Kato, K. Machida, H. Nakanishi and M. Fujita, J. Phys. Soc. Jpn. **59** 1047 (1990). K. Machida and M. Ichioka, J. Phys. Soc. Jpn. **68** 2168 (1999). M. Ichioka and K. Machida, J. Phys. Soc. Jpn. **71** 1836 (2002). E. Kaneshita, M. Ichioka and K. Machida, Phys. Rev. Lett. **88** 115501 (2002).
  - <sup>30</sup> M. Ichioka, M. Takigawa and K. Machida, J. Phys. Soc. Jpn. **70** 33 (2001).
  - <sup>31</sup> M. Takigawa, M. Ichioka and K. Machida, Physica C (in press).
  - <sup>32</sup> M. Takigawa, M. Ichioka and K. Machida, Phys. Rev. Lett. **83** 3057 (1999).
  - <sup>33</sup> M. Takigawa, M. Ichioka and K. Machida, J. Phys. Soc. Jpn. **69** 3943 (2000).
  - <sup>34</sup> D.K. Morr and R. Wortis, Phys. Rev. B **61** R882 (2000).
  - <sup>35</sup> T. Tohyama, S. Nagai, Y. Shibata and S. Maekawa, Phys. Rev. Lett. **82** 4910 (1999).
  - <sup>36</sup> N. Hayashi, M. Ichioka and K. Machida, J. Phys. Soc. Jpn. **67** 3368 (1998).
  - <sup>37</sup> L. Kramer and W. Pesch, Z. Phys. **269** 59 (1974). W. Pesch and L. Kramer, J. Low Temp. Phys. **15** 367 (1974).
  - <sup>38</sup> N. Hayashi, T. Isoshima, M. Ichioka and K. Machida, Phys. Rev. Lett. **80** 2921 (1998).
  - <sup>39</sup> M. Kato and K. Maki, Prog. Theor. Phys. **107** 941 (2001) and M. Kato and K. Maki, Euro. Phys. Lett. **54** 800 (2001).
  - <sup>40</sup> A. Ghosal, C. Kallin, A.J. Berlinsky, Phys. Rev. B **66** 214502 (2002).
  - <sup>41</sup> Y. Tanaka and S. Kashiwaya, private communication.
  - <sup>42</sup> A. Himeda, M. Ogata, Y. Tanaka and S. Kashiwaya, J. Phys. Soc. Jpn. **66** 3367 (1997).
  - <sup>43</sup> K. Kakuyanagi, private communication.